Optical properties of excitons in strained Ga_x In_{1-x} As/GaAs quantum dot: effect of geometrical confinement on exciton *g*-factor

N. R. Senthil Kumar[1], A. John Peter[2*], and Chang Woo Lee[3]

[1]*Department of Physics, RVS School of Engineering College, Dindigul-624 401, India*

[2]*Department of Physics, Govt. Arts College, Melur-625 106, Madurai, India*

[3]*Department of Chemical Engineering and Green Energy Center, College of Engineering, Kyung Hee University, 1Seochun, Gihung, Yongin, Gyeonggi 446-701, Korea*

[*]*Corresponding author: a.john.peter@gmail.com*

Received December 7, 2012; accepted Jun 28, 2013; posted online August 2, 2013

Taking into account anisotropy, nonparabolicity of the conduction band, and geometrical confinement, we discuss the heavy-hole excitonic states in a strained $Ga_xIn_{1-x}As$/GaAs quantum dot for various Ga alloy contents. The strained quantum dot is considered as a spherical InAs dot surrounded by a GaAs barrier material. The dependence of the effective excitonic *g*-factor as a function of dot radius and Ga ion content is numerically measured. Interband optical energy with and without the parabolic effect is computed using structural confinement. The interband matrix element for different Ga concentrations is also calculated. The oscillator strength of interband transitions on the dot radius is studied at different Ga concentrations in the $Ga_xIn_{1-x}As$/GaAs quantum dot. Heavy-hole excitonic absorption spectra are recorded for various Ga alloy contents in the $Ga_xIn_{1-x}As$/GaAs quantum dot. Results show that oscillator strength diminishes when dot size decreases because of the dominance of the quantum size effect. Furthermore, exchange enhancement and exchange splitting increase as exciton confinement increases.

OCIS codes: 250.0250, 250.5590, 160.0160, 160.4760.

doi: 10.3788/COL201311.082501.

Technological progress in the techniques for growing low-dimensional semiconductor crystals has enabled the customization of semiconductor structures toward desired dimensions for specific applications. These techniques include molecular beam epitaxy, metal organic chemical vapor deposition, and electron lithography, which enable the confinement of carriers in one, two, or three dimensions (1D, 2D, or 3D). Because of the reduction in dimensionality of carrier motion, low-dimensional semiconductor systems exhibit unusual properties that can be easily accessible to experimental studies and that lend themselves to theoretical interpretation. Quantum dots, referred to as artificial atoms, are characterized by electron states that take the form of discrete energy levels.

The majority of research has thus far focused on the electronic and optical properties of strained heterostructures under a strain percentage of around 1%. Conversely, studies on experimental data for InAs/GaAs heterostructures that exhibit a lattice mismatch of approximately 7% are scarce. Extensively investigating these highly strained materials is of great interest because of the large splitting between the hh and lh lower bands; such splitting considerably modifies valence band structure. Despite the promising prospects presented by these materials, however, their wide usage is constrained by the limited composition of barrier materials. This composition is responsible for the tunability of the optical band gap of highly strained materials. Doped InAs semiconducting materials present tremendous advantages in spintronic applications because of their large *g*-factor, high-mobility charge carriers, and large spin-orbit interaction[1−3]. The electronic, optical, and magnetic properties of the active regions used for high-performance long-wavelength lasers based on InGaAs semiconducting materials are interesting because low-dimensional InGaAs semiconductors are used on GaAs substrates to develop lasers that range from 1 200 to 1 500 nm. Low-dimensional InGaAs semiconductors are ideal materials given their tremendous temperature stability, high performance, broad high-modulation bandwidths, and low-threshold long wavelengths[4−12]. Moreover, such materials are the preferred light source for wideband optical communications, especially long-term telecommunications applications[4−12]. Zhang *et al.*[13] recently studied the high pulse repetition rates (greater than 10 GHz) of diode-pumped solid-state lasers, which were mode locked using semiconductor saturable absorber mirrors in 1.55-μm InAs/GaAs quantum dots. These quantum dots are extensively applied in laser diodes, optical communications, optical amplifiers, and nonlinear and photonic devices.

Preisler *et al.*[14] conducted photoluminescence excitation spectroscopy under a strong magnetic field to investigate the interband transitions in several ensembles of self-assembled InAs/GaAs quantum dots. The authors determined the excitonic polaron energies and oscillator strengths of interband transitions. Snelling *et al.*[15] studied the Zeeman splitting of the heavy-hole excitons confined in GaAs quantum wells, and other scholars interpreted heavy-hole magneto excitons through the electron-hole exchange interaction induced by confinement[16]. By contrast, the enhancement of the electron-hole exchange interaction induced by 2D confinement is rarely investigated[17].

 © 2013 Chinese Optics Letters

The p-like states in the valence band of InAs semiconductors are strongly coupled to the spin of such valence band; ultimately, total angular momentum is modified, thereby drastically altering the electron g-factor that measures the Zeeman splitting of electron states in the presence of a magnetic field[18]. Sarkar *et al.*[19] conducted a photoluminescence study of the biexciton binding energy and fine-structure splitting in single InAs/AlAs quantum dots. The authors found that binding energy and splitting monotonically decreased as quantum dot emission energy increased. Stranski–Krastanov dots were initially suggested as pyramidal[20], prompting several groups to theoretically investigate the structure of ideal pyramidal dots[21−23]. A theoretical analysis of the mean electron and hole positions in self-assembled InAs-GaAs quantum dot structures has been presented, in which the plane-wave envelope-function technique was used to determine the electronic structures and the measured Stark effect in the structures; these features cannot be explained by assuming a pyramidal dot shape[24]. Using an eight-band strain-dependent k.p Hamiltonian, Pryor[25] calculated the electronic structure of pyramidal-shaped InAs/GaAs quantum dots. The electro-refraction in strained InAs/GaAs and InAs/InP quantum dots has been discussed using a numerical model based on the 4×4 Luttinger-Kohn Hamiltonian theoretically proposed by Prasanth[26], who performed matrix diagonalization with plane-wave basis states and experiments[27].

In this letter, we discuss the heavy-hole excitonic states in a strained $Ga_xIn_{1-x}As/GaAs$ quantum dot at various Ga alloy concentrations. The calculations performed are those on anisotropy, the nonparabolicity of the conduction band, and geometrical confinement. The strained quantum dot is considered a spherical InAs dot surrounded by a GaAs barrier material. The exciton effective Lande factor is measured as a function of dot radius and Ga alloy content in the $Ga_xIn_{1-x}As/GaAs$ quantum dot. Interband emission energy is computed using structural confinement, and the interband matrix element for different Ga concentrations is calculated. The oscillator strength of interband transitions on the dot radius of the InAs/GaAs quantum dot is investigated, and heavy-hole excitonic absorption spectra for various Ga alloy contents in the $Ga_xIn_{1-x}As/GaAs$ quantum dot are recorded.

We consider an exciton in a $Ga_xIn_{1-x}As$ quantum dot surrounded by a spherical potential barrier with GaAs material. We assume a uniform strain in the quantum dot with the general complex of large 3D spatial variations, as in Ref. [28]. The potential inside the dot is assumed to be 0 and that outside is assumed to be V_0. On the basis of the approximation of single-band effective mass, the Hamiltonian of the electron-hole pair in the spherical quantum dot of $Ga_xIn_{1-x}As/GaAs$ can be written as

$$\widehat{H}_{\rm exc} = \sum_{j=e,h}\left(\frac{\vec{p}_j^2}{2m^*_{j(i)}} + V^j\right) - \frac{e^2}{\varepsilon\left|\bar{r}_{\rm e} - \bar{r}_{\rm h}\right|}, \quad (1)$$

where $j = e$, h refer to the electron and hole, respectively; $m^*_{j(i)}$ is the effective mass of the electron (hole), with i referring to the mass of the inner and outer materials; ε is the dielectric constant of the material in the quantum dot; e represents the absolute electron charge; and $|\bar{r}_{\rm e} - \bar{r}_{\rm h}|$ denotes the relative distance between the electron and hole. The strain effects induce an extra potential field, V_{strain}, which we regard as the problem in this letter. For the nanostructure of the strained quantum dot, the confinement potential is considered the sum of the energy offsets of the conduction band (or valence band) and the strain-induced potential in all our calculations.

The electron (hole) confinement potential ($V^j_{\rm conf}$) resulting from the band offset in the $Ga_xIn_{1-x}As/GaAs$ quantum dot structure is given by

$$V^j_{\rm conf} = \begin{cases} 0 & r_j \leqslant R \\ V_0 & r_j > R \end{cases}, \quad (2)$$

where V_0 represents the barrier height. For x =0.2, the barrier heights of the conduction and valence bands are 288 and 192 meV, respectively. The parameter that indicates the offset between the conduction and valence bands is 60:40[29]. The band gap difference between the quantum dot and barrier at Γ-point is given by

$$\Delta E_g^{\Gamma}(x) = 0.359 + 0.491x + 0.58x^2. \quad (3)$$

For any low-dimensional semiconductor system, conduction and valence edge energies are affected primarily by strain contribution, which is introduced in the Hamiltonian through band offset values. Hydrostatic strain influences lattice volume, causing changes in the energy levels of materials. Meanwhile, uniaxial strain causes lattice constant mismatch between two materials.

The strain-induced potential of the conduction band can be expressed as[30]

$$V_{\rm e-strian} = a_{\rm c}(\varepsilon_{xx} + \varepsilon_{yy} + \varepsilon_{zz}), \quad (4)$$

where $a_{\rm c}$ is the deformation potential constant of the conduction band. The strain tensor components are defined as $\varepsilon_{xx} = \varepsilon_{yy} = \frac{a_0 - a}{a}$, where a_0 and a are the lattice parameters of bulk InAs and GaAs, respectively, and $\varepsilon_{zz} = -2\frac{C_{12}}{C_{11}}\varepsilon_{xx}$, where C_{ij} represents the elastic stiffness constants, whose values are given in Table 1.

The strain-induced potential of the valence band can be written as[31]

$$V_{\rm v-strain} = a_{\rm v}(\varepsilon_{xx}+\varepsilon_{yy}+\varepsilon_{zz}) - \frac{b}{2}(\varepsilon_{xx}+\varepsilon_{yy}-2\varepsilon_{zz}), \quad (5)$$

where $a_{\rm v}$ and b are the deformation potential constants of the valence band for the hydrostatic components of the strain along $\langle 001\rangle$.

Internal strain influences electronic parameters and the effective Lande factor. The effective g-factor (which depends on Ga alloy content) of the electron (hole) with an energy $E_{\rm c}(E_{\rm v})$ measured from the bottom (top) of the conduction (valence) band is provided thus[32]

$$g(E,x) = 2 - \frac{2E_{\rm p}(x)\Delta(x)}{3(E_{\rm g}(x)+E)(E_{\rm g}(x)+E+\Delta(x))}, \quad (6)$$

where $E_{\rm g}(x)$ is the Ga-dependent fundamental band gap energy, $\Delta(x)$ is the spin-orbit splitting energy, and $E_{\rm P}$ describes the coupling energy between conduction band Γ_6 and valence bands Γ_7 and Γ_8. The corresponding values are shown in Table 1.

The heavy-hole mass that corresponds to the curvature of the heavy-hole band around Γ is given by

$$\frac{m_0}{m^*_{\rm hh}} = \gamma_1 - 2\gamma_2, \tag{7}$$

where m_0 is the free electron mass, and γ_1 and γ_2 are the Luttinger parameters. The effect of band nonparabolicity is used in our calculations, with the energy-dependent electron mass given as

$$m^*_{\rm NP} = m^*_{\rm e}(1+\alpha E), \tag{8}$$

where α is the material-dependent nonparabolicity parameter ($0.0025\ {\rm meV}^{-1}$)[33] and E is the lowest energy of the electron (hole), obtained by solving the single-particle Schrödinger equation using the electron (hole) bulk mass.

A variational approach is adopted to calculate the binding energy of the 1S state of an exciton as a function of dot radius. The energy levels, wave functions of the bound electron and hole states, and interband emission energy are calculated following Ref. [34]. Thus, exciton binding energy and optical transition energy can be expressed as

$$E_{\rm exc}(x) = E_{\rm e} + E_{\rm h} - \langle H_{\rm exc}\rangle_{\rm min}, \tag{9}$$

$$E_{\rm ph}(x) = E_{\rm e}(x) + E_{\rm h}(x) + E^{\Gamma}_{\rm g}(x) - E_{\rm exc}(x), \tag{10}$$

where $E_{\rm e}$ and $E_{\rm h}$ represent the sum of the lowest binding energy of the electron and hole obtained by self-consistent calculation, respectively; and $E^{\Gamma}_{\rm g}(x)$ is the band gap of the inner dot material. Envelope wave functions and exciton binding energies are considered significant factors in calculating oscillator strength; such calculation is crucial to understanding the absorption spectra recorded during experimentation[35].

Oscillator strength is expressed as

$$f = \frac{E_{\rm p}}{E_{\rm exc}}\Big|\int\limits_V \psi_{\rm exc}(r){\rm d}r\Big|^2, \tag{11}$$

where $E_{\rm exc}$ is the exciton binding energy, $E_{\rm p}$ is the Kane energy of InAs, and $\psi_{\rm exc}$ denotes the exciton wave function. Oscillator strength increases with dot radius. Radiative lifetime can be calculated thus[36]

$$\tau = \frac{2\pi\varepsilon_0 m_0 c^3 h^2}{\sqrt{\varepsilon}e^2 E^2_{\rm exc} f}, \tag{12}$$

where f is the oscillator strength provided by Eq. (11). All the other parameters are universal physical constants.

Oscillator strength and radiative lifetime are two important optical parameters in calculating different linear and nonlinear optical properties. An essential requirement is that the dipole transition that occurs between two energy levels must obey selection rules, such as $\Delta l = \pm 1$, where l is the quantum number of angular momentum. The oscillator strength pertaining to dipole transition is expressed as

$$P_{fi} = \frac{2m*}{\hbar^2}\Delta E_{fi}\left|M_{fi}\right|^2, \tag{13}$$

where ΔE_{fi} is obtained by determining the difference in energy between lower (E_i) and upper (E_f) states. Matrix element $M_{fi} = 2\langle f\left|er\right|i\rangle$ is computed from the electric dipole moment of the transition from the i state to the f state in any low-dimensional semiconductor system. Using the compact matrix approach and Fermi's golden rule, we express total optical absorption as[37]

$$\begin{aligned}\alpha(\omega, I) &= \alpha_1(\omega) + \alpha_3(\omega, I)\\ &= \omega\sqrt{\frac{\mu_0}{\varepsilon_{\rm r}}}Im\left[\varepsilon_0\chi_1(\omega) + \varepsilon_0\chi_3(\omega)I\right],\end{aligned} \tag{14}$$

where μ_0, I, and $\varepsilon_{\rm r}$ are the permeability of the material, the incident light intensity of the electromagnetic field, and the real component of permittivity, respectively. The linear and third-order nonlinear optical absorption coefficients of a quantum dot can be obtained by a density matrix approach, with corresponding expressions given by

$$\alpha_1(\omega) = \frac{4\pi\alpha_f\sigma_{\rm s}}{n_{\rm r}e^2}\hbar\omega\left|M_{fi}\right|^2\delta(E_f - E_i - \hbar\omega). \tag{15}$$

Meanwhile, the nonlinear optical absorption coefficient is given as

$$\begin{aligned}\alpha_3(\omega, I) = &-\frac{32\pi^2\alpha_f\sigma_{\rm s}I}{n^2_{\rm r}e^2\hbar\Gamma_{\rm ff}}\hbar\omega\left|M_{fi}\right|^2\delta(E_f - E_i - \hbar\omega)\\ &\cdot\Big\{1 - \frac{|M_{ff} - M_{ii}|^2}{4|M_{fi}|^2}\\ &\times\frac{[(\hbar\omega - E_{fi})^2 - (\hbar\Gamma_{fi})^2 + 2E_{fi}(E_{fi} - \hbar\omega)]}{E^2_{fi} + (\hbar\Gamma_{fi})^2}\Big\},\end{aligned} \tag{16}$$

where $n_{\rm r}$ is the refractive index of the material examined in this research, $\sigma_{\rm s}$ is the electron density of the quantum dot, ω denotes the angular frequency of incident photon energy, α_f represents the fine structure constant, and E_i and E_f are the confinement energy levels of the ground and first excitation state, respectively. The calculations of excited state energies are adopted from Ref. [38].

On the basis of Eqs. (15) and (16), the energy -conserving delta function approximated by the Lorentzian is given by

$$\delta(E_f - E_i - \hbar\omega) = \frac{\Gamma}{\pi\left\{(E_f - E_i - \hbar\omega)^2 + \Gamma^2\right\}}, \tag{17}$$

where Γ is the line width of the exciton in which Γ=0.1 meV is considered. The homogeneous spectral width resulting from the finite time of coherence between the two energy levels is also taken into account in the calculations.

The exciton binding energy in a spherical $Ga_xIn_{1-x}As/GaAs$ strained quantum dot is numerically calculated using heavy-hole mass because heavy excitons are commonly subjected to experimental investigations. The effect of geometrical confinement is calculated using a finite quantum dot model, in which confinement potential is determined by band offsets and strain effects. We assume a spherical InAs quantum dot embedded in a GaAs material. The variations in the composition x of the quantum dot material modify energy gap. All the material parameters are provided in Table 1. Atomic units are used to determine electronic charges and wave functions; here, we assume that electronic charges and the Planck's constant are unity.

Table 1. Material Parameters* Used in Calculations (All Other Parameters are Linearly Interpolated)

Parameter	InAs	GaAs	Unit
E_g	0.418	1.517	eV
m_e	0.023	0.067	(m_0)
ε	15.15	13.13	
γ_1	20	6.98	
γ_2	8.5	2.06	
C_{11}	83.29	11.88	GPa
C_{12}	45.26	5.38	GPa
C_{44}	23.0	5.94	GPa
a_c	–5.08	–7.17	eV
a_v	1	–1.16	eV
b	–1.8	2	eV
a	0.6058	0.565	nm

*parameters taken from Refs. [54–59].

Figure 1 shows the variations in the binding energy of a heavy-hole exciton of the strained $Ga_xIn_{1-x}As/GaAs$ quantum dot as a function of dot radius for various Ga contents. The inset shows the schematic of the model used in the calculation. As shown in Fig. 2, binding energy decreases as dot radius increases for all Ga contents, a finding attributed to the increase in relative distance between the electron and hole, as well as to the reduction in Coulomb interaction. Conversely, exciton binding energy improves with decreasing dot radius. However, binding energy decreases at small dot sizes because geometrical confinement is governed for smaller dot radii, causing the exciton to become unbound. This finding indicates that quantum dot size has a dominant effect[39,40]. Furthermore, exciton binding energy increases as Ga content increases because the increase in Ga concentration enhances confinement potential. The effect of the attractive Coulomb potential on total energy is also depicted in Fig. 1. Binding energy linearly increases as Ga content increases, a result attributed to the increase in confinement potential with rising Ga concentration. Moreover, small dot radii exhibit sharp variations, but such linear changes gradually occur as dot size increases. This trend is caused by the spatial confinement of nanostructures. Thus, exciton binding energy increases as dimensionality diminishes and excitons are more stable in quantum dots than in bulk materials.

Interband optical energy as a function of dot radius for various Ga concentrations in the strained $Ga_xIn_{1-x}As/GaAs$ quantum dot with and without polaronic mass is shown in Fig. 2. This energy is obtained as the sum of the band gap energy and confinement energies of the electrons and holes minus exciton binding energy. Interband optical energy increases as dot radius decreases for all Ga concentrations because of the confinement of the electron and hole, as well as the increase in Coulomb interaction between them. We determine the exciton binding energy, and consequently, the interband emission energy associated with the Γ band with spatial confinement, allowing for a strong nonparabolicity of the conduction band. The results derived using the bulk (parabolic) mass of the electron and the findings obtained when the effect of band nonparabolicity is considered (Eq. (8)) have been presented. A low interband emission energy is produced when the effect of nonparabolicity is included for the all the dot radii. This result is attributed to the large Coulomb interaction energy when band nonparabolicity is included; moreover, band nonparabolicity enhances the effective mass of electrons[41]. Nonparabolicity more strongly influences large dots and Ga alloy content. As Ga concentration increases in $Ga_xIn_{1-x}As$, so does barrier height. Exciton binding energy increases with Ga concentration in $Ga_xIn_{1-x}As$ because of increasing barrier height. The quantum size effect is illustrated in Fig. 2. Furthermore, interband emission energy increases with Ga concentration, as expected from Eq. (10).

Figure 3 shows the variations in the electron (hole) g -factor as a function of dot radius for various Ga alloy contents in the $Ga_xIn_{1-x}As/GaAs$ quantum dot. The inset shows the variations in effective g-factor as a function of the band gap obtained from the bulk formula[42]. The dot radius approaches 0 and the effective electron (hole) g-factor approaches the bulk g-factor of InAs.

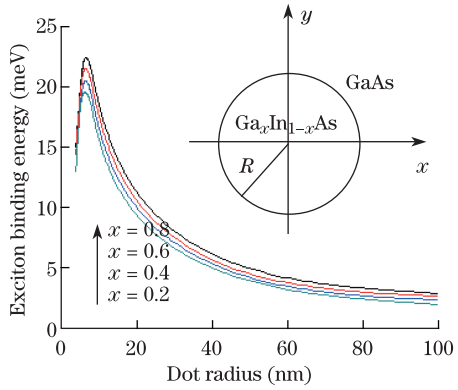

Fig. 1. (Color online) Variations in exciton binding energy as a function of dot radius in the $Ga_xIn_{1-x}As/GaAs$ quantum dot for various Ga contents. The inset shows the schematic of the model used in the calculation.

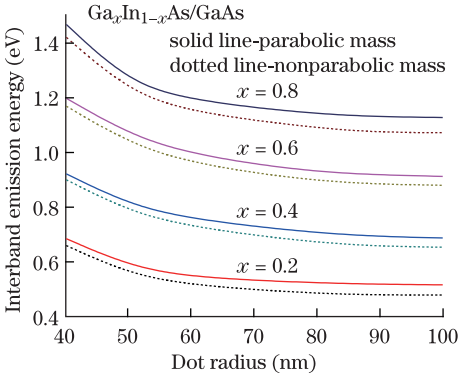

Fig. 2. (Color online) Variations in interband emission energy as a function of dot radius for various Ga concentrations in the $Ga_xIn_{1-x}As/GaAs$ quantum dot with and without parabolic mass.

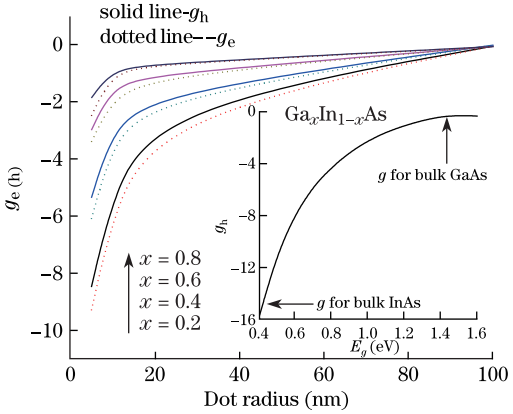

Fig. 3. (Color online) Variations in electron (hole) g-factor as a function of dot radius for various Ga alloy contents in the $Ga_xIn_{1-x}As/GaAs$ quantum dot. The inset shows the variations in effective g-factor as a function of band gap.

By contrast, the g-factor approaches the bulk g-factor of GaAs in large dots. The effective electron (hole) g-factor increases not only with increasing dot radius, but also with increasing Ga alloy content[43]. The magnitude of the hole g-factor is larger than that of the electron g-factor. No direct means of measuring the electron (hole) g-factor in InGaAs quantum dots is currently available, but this behavior is consistent with the trend of the bulk g-factor. The g-factor of the conduction band in bulk semiconductors is given by[42,44,45]

$$g = 2 - \frac{2E_p\Delta}{3E_g(E_g + \Delta)}, \tag{18}$$

where E_g and Δ are the band gap energy and spin-orbit splitting energy, respectively. E_P is the Kane energy that describes S- and P-like block functions. Equation (18) yields poor results because strain is excluded from the calculation. Thus, the decrease in the g-factor with quantum dot size demonstrates the effect of geometrical confinement.

Figure 4 shows the variations in theoretical exchange enhancement as a function of dot radius for various Ga concentrations in the strained $Ga_xIn_{1-x}As/GaAs$ quantum dot. The inset illustrates the variations in exchange splitting as a function of dot radius in the $Ga_xIn_{1-x}As/GaAs$ quantum dot for various Ga alloy contents. The exchange enhancement of J with respect to the bulk value of the exciton in the quantum dot is demonstrated by considering the overlap integral between the electron and hole wave function in the exciton, with the inclusion of two parametric variational parameters. Exchange enhancement monotonically increases as dot radius decreases. A sudden decrease in exchange enhancement occurs for small dot radii because of penetration into the barrier material. Similar trends have been previously observed for GaAs and InGaAs quantum wells[46]. Exchange enhancement increases as exciton confinement intensifies. The inset in Fig. 4 shows heavy-hole exchange splitting as a function of dot radius for various Ga alloy contents in the strained $Ga_xIn_{1-x}As/GaAs$ quantum dot. Exchange splitting energy increases as dot radius decreases. The energy is more pronounced in small dots and increases with alloy content because of the strain contribution and geometrical confinement of small dots; the results qualitatively resemble those of a previous investigation[47].

Figure 5 shows the variations in oscillator strength as a function of dot radius for various Ga alloy contents in the strained $Ga_xIn_{1-x}As/GaAs$ quantum dot. Oscillator strength increases with dot radius, whereas exciton radiative lifetime decreases with dot radius. Oscillator strength intensifies as Ga concentration in the InGaAs/GaAs quantum dot decreases, suggesting that small effective masses result in large oscillator strength. Moreover, as indicated in Eqs. (12) and (13), oscillator strength depends purely on effective mass. Thus, oscillator strength is expected to decrease as the quantum size effect dominates.

Figure 6 shows the variations in the total absorption coefficient of an exciton in a spherical quantum dot with a dot radius of 5 nm as a function of photon energy for different values of Ga alloy content in the strained $Ga_xIn_{1-x}As/GaAs$ quantum dot, with I =10 MW/m^2. The inset shows the resonant absorption coefficient as a function of Ga alloy content. The absorption coefficient peak moves to a higher photon energy as Ga alloy content increases, suggesting that the increase in Ga concentration shifts resonance toward the blue region in the quantum dot. This phenomenon is caused by the

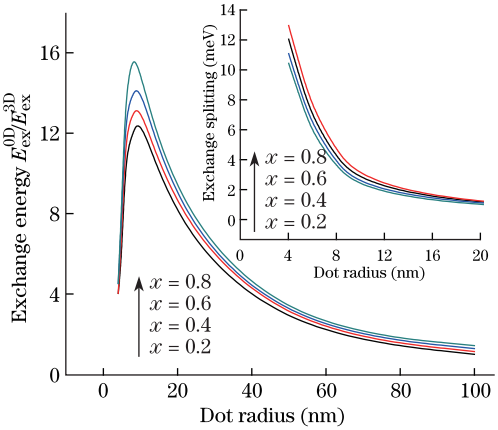

Fig. 4. (Color online) Variations in theoretical exchange enhancement as a function of dot radius for various Ga concentrations in the strained $Ga_xIn_{1-x}As/GaAs$ quantum dot. The inset shows the variations in exchange splitting as a function of dot radius in the $Ga_xIn_{1-x}As/GaAs$ quantum dot for various Ga alloy contents.

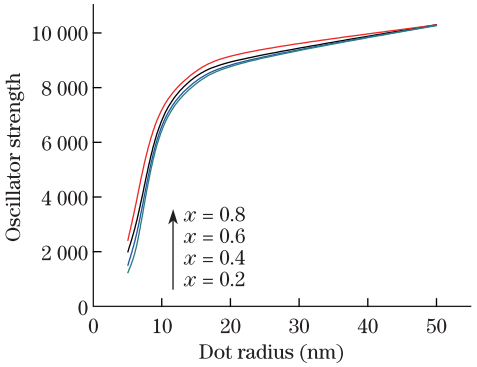

Fig. 5. (Color online) Variations in oscillator strength as a function of dot radius for various Ga alloy contents in the strained $Ga_xIn_{1-x}As/GaAs$ quantum dot.

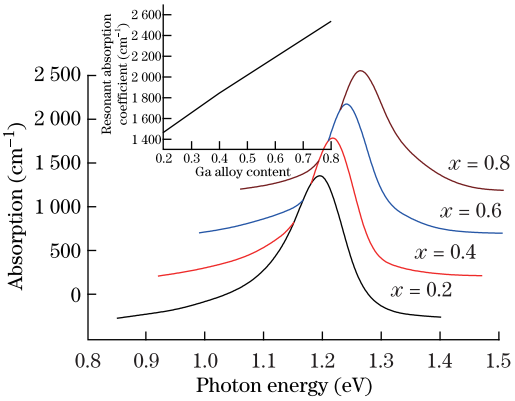

Fig. 6. (Color online) Variations in the total absorption coefficient of an exciton in a spherical quantum dot with a dot radius of 5×10^{-9} m as a function of photon energy for different values of Ga alloy contents in the strained $Ga_xIn_{1-x}As/GaAs$ quantum dot. The inset shows the resonant absorption coefficient as a function of Ga alloy content.

increase in spacing between energy levels when Ga content is added[48]. Moreover, the application of Ga alloy content in the InGaAs quantum dot modifies barrier height and lattice constant, which are related to the energy gap of energy levels when the Coulomb potential between the electron and hole are considered. Furthermore, the magnitude of the total linear absorption coefficient shifts toward high energies (blue shift) because of the incorporation of Ga concentration. The transition matrix element, electron density, and certain optical properties depend on the geometrical shape of a quantum dot. As shown in Fig. 6, the linear absorption coefficient is large because of the positive linear susceptibility term; the α_3 governed by the third-order nonlinear susceptibility term is negative. Therefore, the total absorption coefficient significantly decreases, as determined according to Eq. (14), in which these two effects are combined. Nevertheless, the contribution from the nonlinear optical absorption coefficient should be considered under a very strong optical intensity.

The matrix dipole moment and energy levels should be considered when investigating oscillator strength. A large dipole matrix element is obtained when the energies of photons are equal to the intersubband transition energies in a system. This property is important for nonlinear optical properties, such as the index of refraction and absorption coefficient. Optical properties are also enhanced. Our results coincide with those of previous investigations on the analytical forms of the changes in absorption coefficients and related intersubband optical transitions with incident optical intensity. The inset in Fig. 6 shows that the resonant absorption coefficient linearly varies as Ga alloy content increases for all the dot radii and that the resonant absorption coefficient is large at small dot radii. These results are attributed to the increase in exciton binding energy when dot radius decreases. These findings are similar to earlier experimental investigations[49].

In conclusion, the heavy-hole excitonic states in a strained $Ga_xIn_{1-x}As/GaAs$ quantum dot for various Ga alloy contents are discussed, with the consideration for anisotropy, the nonparabolicity of the conduction band, and geometrical confinement. The dependence of the effective excitonic g-factor as a function of dot radius on Ga alloy content is numerically calculated. The dependence of excitonic binding energy on dot radius is elucidated. The interband matrix element for different Ga concentrations is also computed. The oscillator strength of interband transitions on the dot radius of the InAs/GaAs quantum dot is discussed, and the heavy-hole excitonic absorption spectra for various Ga alloy contents in the $Ga_xIn_{1-x}As/GaAs$ quantum dot are recorded. We assume a single heavy-hole valence band, in which the valence band mixing effect is disregarded. However, the effects of valence band mixing and carrier screening are crucial to studies on nanostructures[50−53]. The crossover between hh and lh subbands is a noteworthy subject for future studies, in which the performance of semiconductor lasers and electro-optic modulators can be improved by tailoring the valence band structure via strain contribution.

References

1. D. Grundler, Phys. Rev. Lett. **84,** 6074 (2000).
2. Vurgaftman, J. R. Meyer, and L. R. Ram-Mohan, J. Appl. Phys. **89,** 5815 (2001).
3. C. H. Möller, C. Heyn, and D. Grundler, Appl. Phys. Lett. **83,** 2181 (2003).
4. N. F. Massé, E. Homeyer, O. Dehaese, R. Piron, F. Grillot, and S. Loualiche, Appl. Phys. Lett. **91**, 131113 (2007).
5. L. Li, G. Liu, Z. Li, M. Li, X. Wang, Y. Qu, and B. Bo, Chin. Opt. Lett. **7,** 741 (2009).
6. D. H. Zhang, Chin. Opt. Lett. **3,** 455 (2005).
7. G. T. Liu, A. Stintz, H. Li, K. J. Malloy, and L. F. Lester, Electron. Lett. **35,** 1163 (1999).
8. O. B. Shchekin and D. G. Deppe, IEEE Photon. Technol. Lett. **14,** 1231 (2002).
9. G. Ozgur, A. Demir, and D. G. Deppe, IEEE J. Quantum Electron. **45,** 1265 (2009).
10. N, Tansu, J.-Y. Yeh, and L. J. Mawst, J. Phys.: Condens. Matter **16,** S3277 (2004).
11. N. Tansu, J.-Y. Yeh, and L. J. Mawst, IEEE J. Quantum Electron. **9,** 1220 (2003).
12. N. Tansua and L. J. Mawst, J. Appl. Phys. **97,** 054502 (2005).
13. Z. Y. Zhang, A. E. H. Oehler, B. Resan, S. Kurmulis, K. J. Zhou, Q. Wang, M. Mangold, T. Süedmeyer, U. Keller, K. J. Weingarten, and R. A. Hogg, Scientific Reports **2,** 477 (2012).
14. V. Preisler, T. Grange, R. Ferreira, L. A. de Vaulchier, Y. Guldner1, F. J. Teran, M. Potemski, and A. Lemaitre, AIP Conf. Proc. **893,** 985 (2007).
15. M. J. Snelling, E. Blackwood, C. J. McDonagh, R. T. Harley, and C. T. B. Foxon, Phys. Rev. B **45,** 3922 (1992).
16. F. M. Munteanua, Y. Kima, C. H. Perryb, D. G. Rickela, J. A. Simmonsc, and J. L. Reno, Solid State Commun. **114,** 63 (2000).
17. Y. Chen, B. Gil, P. Lefebvre, and H. Mathieu, Phys. Rev. B **37,** 6429 (1988).
18. W. Sheng and A. Babinski, Phys. Rev. B. **75,** 033316 (2007).
19. D. Sarkar, H. P. van der Meulen, J. M. Calleja, J. M. Becker, and R. J. Haug, J. Appl. Phys. **100,** 023109 (2006).

20. M. Grundmann, O. Stier, and D. Bimberg, Phys. Rev. B **52,** 11969 (1995).
21. K. Chang and J.-B. Xia, Solid State Commun. **104,** 351 (1997).
22. A. J. Williamson and A. Zunger, Phys. Rev. B **59,** 15819 (1999).
23. M. A. Cusack, P. R. Briddon, and M. Jaros, Phys. B: Condens. Matter **253,** 10 (1998).
24. J. A. Barker and E. P. O'Reilly, Phys. Rev. B **61,** 13840 (2000).
25. C. Pryor, Phys. Rev. B **57,** 7190 (1998).
26. R. Prasanth, J. Appl. Phys. **99,** 054501 (2006).
27. R. Prasanth, J. E. M. Haverkot, A. Deepthy, E. W. Bogaart, J. J. G. M. van der Tol, E. A. Patent, G. Zhao, Q. Gong, P. J. van Veldhoven, R. Nötzel, and J. H. Wolter, Appl. Phys. Lett. **84,** 4059 (2004).
28. D. P. Williams, S. Schulz, A. D. Andreev, and E. P. O'Reilly, IEEE J. Sel. Top. Quantum Electron. **15,** 1092 (2009).
29. E. H. Li, Physica E: Low-Dimensional Systems and Nanostructures **5,** 215 (2000).
30. J. Singh, *Optoelectronics*: *An Introduction to Materials and Devices* (Tata McGraw Hill, New Delhi, 1996).
31. G. L. Bir and E. Pikus, *Symmetry and Strain-Induced Effects in Semiconductors* (Wiley, New York, 1974).
32. T. Ito, W. Shichi, Y. Okami, M. Ichida, H. Gotoh, H. Kamada, and H. Ando, Phys. Stat. Sol. C **6,** 319 (2009).
33. J. Scriba, C. Gauer, A. Wixfoith, L. Kotthaus, C. Bolognesi, C. Nguyen, and H. Kroemer, Sol. St. Coram. **86,** 633 (1993).
34. M. Narayanan and A. J. Peter, Phys. B: Condens. Matter **407,** 433 (2012).
35. E. A. Muljarov, A. L. Yablonskii, S. G. Tikhodeev, A. E. Bulatov, and J. L. Birman, J. Math. Phys. **41,** 6026 (2000).
36. A. Vladimir, Fonoberov, and A. A. Balandin, Appl. Phys. Lett. **85,** 5971 (2004).
37. J. S. de Sousa, J.-P. Leburton, V. N. Freire, and E. F. da Silva, Jr., Phys. Rev. B **72,** 155438 (2005).
38. G. Murillo, J. C. Arce, C. A. Duque, and N. Porras-Montenegro, Phys. Stat. Sol. C **4,** 360 (2007).
39. N. Arunachalam, A. J. Peter, and C. K. Yoo, J. Lumin. **132,** 1311 (2012).
40. R. T. Senger and K. K. Bajaj, Phys. Rev. B **68,** 205314 (2003).
41. Y. Sidor, B. Partoens, F. M. Peeters, J. Maes, M. Hayne, D. Fuster, Y. Gonzalez, L. Gonzalez, and V. V. Moshchalkov, Phys. Rev. B **76,** 195320 (2007).
42. C. E. Pryor and M. E. Flatté, Phys. Rev. Lett. **96,** 026804 (2006).
43. G. Hendorfer and J. Schneider, Semicond. Sci. Technol. **6,** 595 (1991).
44. S. Zwerdling, B. Lax, L. M. Roth, and K. J. Button, Phys. Rev. **114,** 80 (1959).
45. L. M. Roth, B. Lax, and S. Zwerdling, Phys. Rev. **114,** 90 (1959).
46. Y. Chen, B. Gil, P. Lefebvre, and H. Mathieu, Phys. Rev. B **37,** 6429 (1988).
47. K. M. Kumar, A. J. Peter, and C. Lee, Euro. Phys. J. B **11,** 23 (2011).
48. ÍKarabulut and S. Baskoutas, J. Appl. Phys. **103,** 073512 (2008).
49. S. Liang and W. Xie, Phys. B: Condens. Matter **406,** 2224 (2011).
50. S. W. Corzine, R. H. Yan, and L. A. Coldren, Appl. Phys. Lett. **57,** 2835 (1990).
51. S. L. Chuang, Phys. Rev. B **43,** 9649 (1991).
52. H. P. Zhao, G. Y. Liu, X. H. Li, R. A. Arif, G. S. Huang, J. D. Poplawsky, and S. T. Penn, IEEE J. Quantum Electron. **45,** 66 (2009).
53. H. P. Zhao, G. Liu, and N. Tansu, J. Appl. Phys. **104,** 043104 (2008).
54. D. D. Nolte, W. Walukiewicz, and E. E. Haller, Phys. Rev. Lett. **59,** 501 (1987).
55. S. Adachi, J. Appl. Phys. **53,** 8775 (1992).
56. M. P. C. Krijn, Semicond. Sci. Technol. **6,** 27 (1991).
57. S. H. Wei and A. Zunger, Phys. Rev. B **60,** 5404 (1999).
58. M. D. Frogley, J. R. Downers, and D. J. Dunstan, Phys. Rev. B **62,** 13612 (2000).
59. C. A. Duque, N. Porras-Montenegro, Z. Barticevic, M. Pacheco, and L. E. Oliveira, Phys. B: Condens. Matter **18,** 1877 (2006).